Review

Physical image quality metrics for the characterization of X-ray machines used in fluoroscopy-guided pediatric cardiac interventional procedures

Diego Nocetti *, Kathia Villalobos , Kevin Wunderle

Posted Date: 8 August 2023

doi: 10.20944/preprints202308.0657.v1

Keywords: Image quality; interventional radiology; pediatrics

Review

Physical Image Quality Metrics for the Characterization of X-ray Machines Used in Fluoroscopy-Guided Pediatric Cardiac Interventional Procedures

Diego Nocetti [1,*], Kathia Villalobos [1] and Kevin Wunderle [2]

[1] Departamento de Tecnología Médica, Facultad de Ciencias de la Salud, Universidad de Tarapacá; dnocetti@academicos.uta.cl; kathia.villalobos.olivares@gmail.com
[2] Department of Radiology, Cleveland Clinic, Cleveland, OH, US; wunderk@ccf.org
* Correspondence: dnocetti@academicos.uta.cl

Abstract: Pediatric interventional cardiology procedures are essential in diagnosing and treating congenital heart disease in children; however, they raise concerns about potential radiation exposure. Managing radiation doses and assessing image quality in angiographs becomes imperative for safe and effective interventions. This study aims to comprehensively analyze the current understanding of physical image quality metrics relevant for characterizing X-ray machines used in fluoroscopy-guided pediatric cardiac interventional procedures, considering the main factors reported in the literature that influence this outcome. A search in Scopus and Web of Science, using relevant keywords and inclusion/exclusion criteria, yielded fourteen relevant articles published between 2000 and 2022. The physical image quality metrics reported were noise (N), signal-to-noise ratio (SNR), contrast (C), contrast-to-noise ratio (CNR) and high contrast spatial resolution (HCSR). Various factors influencing image quality were investigated, such as PMMA thickness, operation mode, anti-scatter grid presence and tube voltage. Objective evaluations using these metrics ensure impartial assessments for main factors affecting image quality, improving in the characterization fluoroscopic X-ray machines, and aiding informed decisions to safeguard pediatric patients during procedures.

Keywords: image quality; interventional radiology; pediatrics

1. Introduction

Interventional cardiology procedures constitute a substantial source of medical radiation exposure globally, with the potential to subject patients to significant radiation levels [1]. This concern is particularly relevant for pediatric patients with congenital heart disease, as they may necessitate multiple imaging studies, such as cardiac catheterization, which can extend examination durations and elevate radiation exposure [2]. Notably, there has been a noteworthy upsurge in the prevalence of prolonged pediatric cardiac interventions, further accentuating the risk of radiation exposure in this population [3].

Children are inherently more vulnerable to the adverse effects of radiation due to their higher radiosensitivity, which is influenced by factors such as their cell proliferation rate and abundance of undifferentiated cells, rendering them more susceptible to genetic damage from radiation [2]. Furthermore, considering the longer potential lifespan of children during which neoplasms may develop, their risk of radiation-induced cancer is elevated [1,4]. Studies have shown that radiation exposure in children under the age of 15 years is two to three times more likely to lead to cancer compared to adults, highlighting the heightened risk in younger age groups [5–7]. Hence, it becomes imperative to carefully assess and optimize radiation doses and image quality for pediatric patients undergoing interventional cardiology procedures [3,8,9].

 doi:10.20944/preprints202308.0657.v1

Evaluating the radiation dose rates and image quality of X-ray systems utilized in pediatric interventional procedures is of paramount importance to strike a balance between optimal image quality and appropriate doses for these patients [10]. However, the complexity of these systems, which encompass diverse models, technologies, and operational modes, can pose challenges for cardiologists when comparing and selecting the most suitable options for a given procedure and patient size [2,11]. Thoroughly characterizing X-ray systems used in pediatric interventional procedures using appropriate phantoms and test objects is essential to optimize procedures and guide the selection of protocols and operation modes, ensuring adequate image quality while minimizing radiation exposure to the lowest reasonably achievable levels [1,2,8,11]. This physical characterization can provide valuable data to improve procedures and facilitate informed decisions in selecting protocols and operation modes [10,11].

In that sense, image quality assessment can be conducted using subjective and objective approaches. Subjective evaluation, however, may be influenced by factors such as observer performance, monitor configuration, and ambient lighting, leading to notable discrepancies among observers and inconsistencies in quality control. To ensure an impartial evaluation of image quality, a DICOM viewer can be employed, enabling measurements of average and standard deviation within multiple regions of interest (ROIs). This method proves valuable in assessing image quality during acceptance tests, determining appropriate action or suspension levels, and establishing reference values for constancy evaluations [9].

Within this framework, image quality metrics commonly considered are signal-to-noise ratio (SNR) [1,5,12–14], contrast-to-noise ratio (CNR) [9–11,14] and high contrast spatial resolution (HCSR) [6,8,11,12]. These metrics can help to optimize the settings of X-ray systems for different patient sizes, ensuring comparable image quality while minimizing patient radiation doses [11]. By utilizing these objective measures, healthcare professionals can make informed decisions regarding the selection of protocols and operation modes for pediatric interventional procedures, prioritizing patient safety and achieving optimal imaging outcomes.

This systematic review aims to provide a comprehensive analysis of the current understanding of physical image quality metrics relevant to X-ray machines in pediatric interventional cardiology, considering the main factors reported in the literature that influence this outcome. The review addresses the following research questions (RQs):

- RQ 1: What are the primary physical image quality metrics commonly utilized for characterizing X-ray machines employed in fluoroscopy-guided pediatric interventional cardiac procedures, and what are the prevalent methods employed to measure these metrics?
- RQ 2: What factors have been examined in the literature for their impact on physical image quality metrics in characterizing X-ray machines used in fluoroscopy-guided pediatric interventional cardiac procedures?

Through a comprehensive analysis of the responses to these research questions, this study endeavors to illuminate the present understanding of physical image quality met- rics applicable to X-ray machines in pediatric interventional cardiology. The findings from this review will offer valuable insights that can benefit clinical practice and guide future research endeavors in this domain.

2. Materials and Methods

Between March and April 2023, a systematic literature review was conducted, utilizing Scopus and Web of Science as the main sources of information. The search strategy incorporated relevant descriptors, including image quality, signal-to-noise ratio, contrast-to-noise ratio, spatial resolution, pediatric, interventional, and cardiology. The search filters were narrowed to primary articles in English and Spanish, with publication dates ranging from 2000 to 2022.

To be included in the review, articles had to meet specific criteria: (i) they evaluated image quality using physical metrics, (ii) focused on characterizing X-ray machines employed in fluoroscopy-guided cardiac interventional procedures, and (iii) involved pediatric patients. Exclusion criteria comprised irrelevant topics, descriptive articles, literature reviews, studies conducted using other imaging techniques or involving adult patients, those lacking objective

 doi:10.20944/preprints202308.0657.v1

evaluation of image quality, and those inaccessible in full text. The article selection process followed the guidelines outlined by the PRISMA initiative [16], and it was performed in four stages, as depicted in Figure 1.

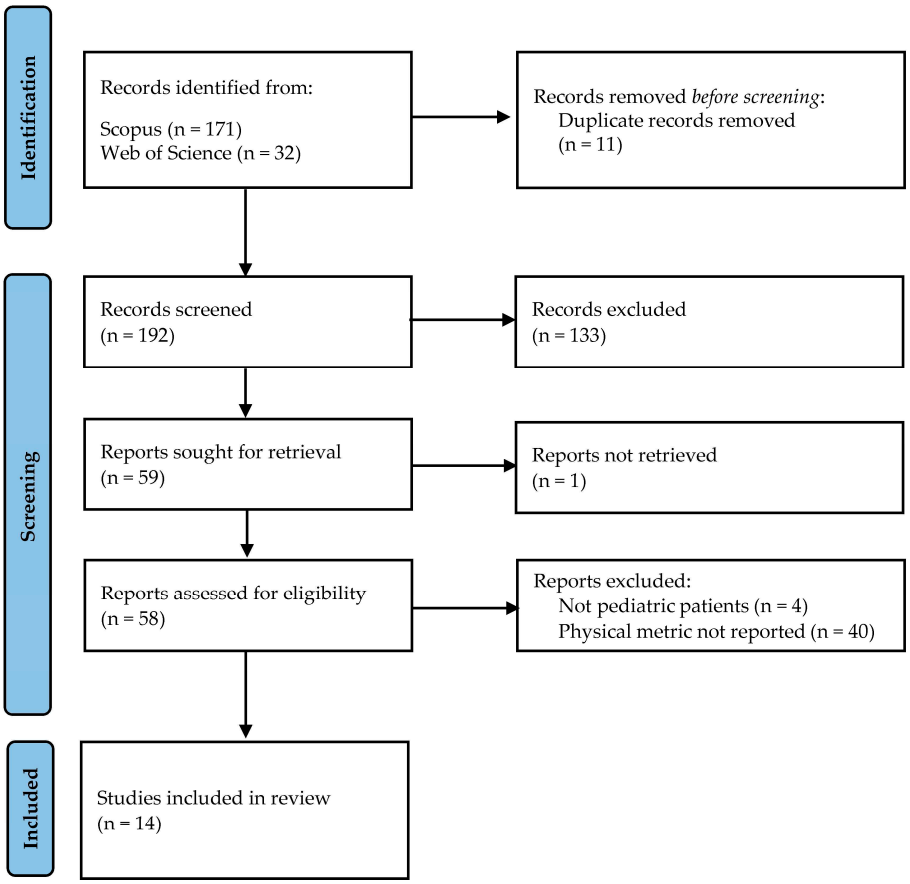

Figure 1. Flowchart of the article selection process in the current systematic review following the PRISMA initiative [16].

Following the removal of duplicates, the authors conducted an individual review of titles and abstracts, engaging in discussions to reach conclusions. In cases of agreement, the articles proceeded to the next stage; otherwise, the relevance of the work was further discussed before making a final decision. Upon consensus on the articles to be included, the authors independently read the full-text and categorized the information based on the evaluated quality metric, method employed for objective image quality assessment, angiographic system, factors influencing image quality and main findings of each report. The authors then compared their decisions regarding the included articles, and any discrepancies were resolved through further discussion. Ultimately, a total of 14 articles were selected for the final analysis.

3. Results

We conducted a systematic review of physical image quality metrics for X-ray machines used in fluoroscopy-guided pediatric interventional procedures. After screening, 14 studies (published between 2000 and 2022) met the inclusion criteria.

3.1. Physical image quality assessment

Table 1 displays the selected studies obtained from the search strategy. The table provides essential details, including the last name of the first author, physical image quality metric, test object assessed, software used for objective evaluation, number of frames analyzed, matrix size and bit

Preprints (www.preprints.org) | NOT PEER-REVIEWED | Posted: 8 August 2023 doi:10.20944/preprints202308.0657.v1

depth. The most frequently reported metric was SNR (n=10), followed by HCSR (n=8). Additionally, C (n=3) and CNR (n=3) were also reported, while N and SdNR appeared in a smaller number of studies (n=1 each).

Table 1. Selected studies using the search strategy, considering the analyzed physical image quality metrics and other methodological aspects.

First author (reference)	Image quality metric	Test object	Software	No. images analyzed (frames)	Matrix size (bit depth)
Ubeda *et al*. [1]	SNR, HCSR	TOR 18FG	Osiris 4.19	3 (10, 12, 15)	512×512 (8 bits)
Bor *et al*. [12]	SNR, C, HCSR	LCD4 Hüttner type 18	N.R.	N.R.	N.R.
De las Heras *et al*. [9]	CNR	IEC type B	N.R.	N.R.	N.R.
Corredoira *et al*. [13]	SNR, HCSR	TOR 18FG	ImageJ 1.48r	3 (5, 8, 10)	1,024×1,024 (12 bits)
Lubis *et al*. [5]	SNR	In-house	ImageJ	1 (random)	N.R.
Ubeda *et al*. [2]	SNR	TOR 18FG	Osiris 4.18	3 (10, 12, 15)	1,024×1,024 512×512 (8 bits)
Ubeda *et al*. [4]	SNR, HCSR	TOR18FG	Osiris 4.18	3 (10, 12, 15)	512×512 (8 bits)
Kordolaimi *et al*. [15]	SNR	5 mm-thick aluminum plate; TOR 18FG	N.R.	N.R.	N.R.
Ubeda *et al*. [8]	SNR, HCSR	TOR 18FG	Osiris 4.18	3 (10, 12, 15)	512×512 (8 bits)
Vañó *et al*. [17]	SNR, HCSR	TOR 18FG	Osiris 4.18	3 (10, 12, 15)	1,024×1,024 (12 bits) 512×512 (8 bits)
Vañó *et al*. [6]	N, SdNR, HCSR	TOR 18FG	Osiris 4.18	3 (5, 8, 10)	512×512 (8 bits)
Gislason *et al*. [10]	C, CNR	Tin detail	Matlab R2008A	40 (1-40)	N.R.
Vañó *et al*. [11]	SNR, C, CNR, HCSR	TOR 18FG	Osiris 4.18	3 (5, 8, 10)	512×512 (8 bits)
Onnasch *et al*. [7]	SNR	Patient images	N.R.	1 (1)	512×512 (8 bits)

SNR, signal-to-noise ratio; HCSR, high contrast spatial resolution; C, contrast; CNR, contrast-to-noise ratio; N, noise; SdNR, signal difference-to-noise ratio. N.R., data not reported.

3.2. Equations utilized for physical image quality metrics calculation

In this section, we present the equations utilized for calculating the physical image quality metrics.

3.2.1. N objective estimation

Objective N estimation involved measuring the standard deviation value (SD_{Bg}) and the mean value (Bg) of the pixels within a ROI located in the proximity of the target structure (e.g., the first low-contrast disk of the test object). This metric was calculated using the Eq. 1 [6]:

$$N = \frac{SD_{Bg}}{Bg} \quad (1)$$

3.2.2. SNR objective estimation

Preprints (www.preprints.org) | NOT PEER-REVIEWED | Posted: 8 August 2023 doi:10.20944/preprints202308.0657.v1

Next, we present the most frequently used equation for calculating the SNR in pediatric interventional cardiology equipment [1,2,5,8,11,13,15,17].

$$SNR = \frac{Bg - ROI}{\sqrt{\frac{SD_{Bg}^2 + SD_{ROI}^2}{2}}} \quad (2)$$

Where ROI and Bg correspond to the average value of the pixels contained in an ROI located in an object of interest of higher attenuation than the surrounding structures (background) and to the background, respectively. While SD_{ROI} and SD_{Bg} to the standard deviation of the pixels contained in the same ROIs.

In the study by Bor *et al*., they utilized a formula based solely on the averages of both the region of interest and the background [12].

$$SNR = \frac{ROI - Bg}{\sqrt{ROI + Bg}} \quad (3)$$

Finally, one parameter derived from the SNR is the SdNR, whose formula retains the numerator of Eq. 2 but replaces the denominator with the SD_{Bg} [6].

3.2.3. C objective estimation

The formula used to determine C is as follows [10,11]:

$$C = \frac{Bg - ROI}{Bg} \quad (4)$$

Where ROI and Bg represent the average pixel value within an object of interest with higher attenuation than the surrounding structures (background) and the background itself, respectively.

Alternatively, one of the evaluated articles employed the same structure but interchanged the order of the subtraction in the numerator of the fraction [12].

3.2.4. CNR objective estimation

The three articles reporting this metric in the context of pediatric interventional cardiology used different formulas, which are presented below:

$$CNR = \frac{ROI - Bg}{SD_{Bg}} \quad (4)$$

In the Eq. (4), extracted from article [9], ROI represents the average pixel value within an object of interest that has higher attenuation than the background, while Bg corresponds to the mean value of the background itself. SD_{Bg} denotes the standard deviation of the pixels belonging to the background.

The article by Vañó *et al*. proposes a formula based on the mean values of the object of interest (ROI) and the background (Bg) [11], resulting in the Eq. (5):

$$CNR = \frac{Bg - ROI}{Bg^2} \quad (5)$$

Finally, in the article [10] the CNR was evaluated using the formula reported for SNR in the literature, as shown in Eq. 2.

3.2.5. HCSR objective estimation

Preprints (www.preprints.org) | NOT PEER-REVIEWED | Posted: 8 August 2023 doi:10.20944/preprints202308.0657.v1

The equation utilized in literature to calculate HCSR [1,4,6,8,11–13,17] is provided below:

$$HCSR = SD_1 - SD_2 \quad (6)$$

SD_1 denotes the standard deviation of the pixel value within a region inside the bar pattern, typically the seventh group of bars within the TOR 18FG, while SD_2 corresponds to the background within the region of higher attenuation on the bar pattern.

3.3. Factors influencing image quality

Table 2 provides an overview of the factors and categories investigated by each selected article obtained from the employed search strategy.

Table 2. Selected studies from the search strategy. Reference, fluoroscopic system, detector system, factors, and categories influencing physical image quality studied by each article.

Reference	Fluoroscopic system (detector)	Factor	Categories
[1]	Siemens Artis Zee-Zeego (FPD)	PMMA thickness	4, 8, 12, 16, 20 cm
		Operation mode	FL, FM, FH, CI
[12]	Prototype (FPD)	PMMA thickness	5, 10, 15, 20, 25 cm
		Anti-scatter grid	With 8:1 and 12:1 covered with carbon fiber, 10:1 and 12:1 covered with aluminum, or without grid
		Tube voltage	70, 90, 120 kV
[9]	Philips Allura FD 20/10 (FPD)	PMMA thickness	5.7, 25.7 cm
[13]	Siemens Artis Zee VC14 (FPD)	Tube voltage	4, 8, 12, 16, 20 cm
		Field of view	22, 32, 42, 48 cm
[5]	Philips Allura Xper FD10 (FPD)	Operation mode	FL, FM, FH, CI
		Vessel diameter	0.1, 0.2, 0.4, 0.6, 0.8 cm
		Frames per second	15, 30 fps
		Contrast mode	Low, high
[2]	Siemens Axiom Artis BC (II)	PMMA thickness	4, 8, 12, 16, 20 cm
		Operation mode	FL, FM, FH, CI
[4]	Siemens Axiom Artis BC (II)	PMMA thickness	4, 8, 12, 16 cm
		Operation mode	FL, FM, FH, CI
[15]	Innova 2100 IQ (FPD)	Anti-scatter grid	With or without
		PMMA thickness	5, 10, 15, 20 cm
	Advantx e E/LC þ DLX (II)	Field of view	12, 15, 17, 20 cm
[8]	Siemens Axiom Artis dBC (FPD)	PMMA thickness	4, 8, 12, 16 cm
	Philips Allura Xper FD20 (FPD)	Operation mode	FL, FM, FH, CI
	Toshiba Rebuilt (II)		
	Siemens Axiom Artis BC (II)		
	General Electric Advantx (II)		
[17]	Siemens Axiom Artis dBC (FPD)	PMMA thickness	16, 20, 24, 28 cm
	Siemens Axiom Artis FC (II)	Matrix size	512×512, 1,024×1,024
[6]	Siemens Axiom Artis dBC (FPD)	PMMA thickness	8, 12, 16 cm
	Siemens Axiom Artis BC (II)	Fluoroscopic system	FPD, II
[10]	Allura FD10 (FPD)	PMMA thickness	8.5, 12, 16 cm
		Anti-scatter grid	With or without
		Tube voltage	50, 55, 60, 65, 70 kV
[11]	Siemens Axiom Artis BC (II)	PMMA thickness	4, 8, 12, 16, 20 cm
		Operation mode	FL, FM, FH, CI
		Field of view	16, 22

[7]	Philips Integris BH 5000 (II)	PMMA thickness	8, 11, 15.5, 18.5 cm
		Anti-scatter grid	With or without
		Tube voltage	50 – 90 kV
		Filter thickness	0.2, 0.4 mmCu
		AEC program	Program (P) from 1 to 6

FPD, flat panel detector; II, image intensifier; PMMA, polymethyl methacrylate; AEC, automatic exposure control; FL, low fluoroscopy dose; MD, medium fluoroscopy dose; HD, high fluoroscopy dose; CI, cine; fps, frames per second.

4. Discussion

Characterizing angiographic equipment for pediatric use is of utmost importance, given the intricacy of X-ray systems in pediatric interventional procedures [2]. This characterization entails assessing dose and image quality using diverse techniques, such as ESAK measurement and image quality assessment with test objects. Such evaluations enable cardiologists to identify optimal protocols and operation modes that strike a balance between image quality and dose, thereby minimizing potential long-term tissue damage in vulnerable pediatric patients [1,10]. Additionally, this evaluation facilitates the selection of appropriate operation modes for different procedures and patient sizes, ensuring the safe and effective use of fluoroscopy-guided pediatric cardiac interventions [11].

The objective of this article is to offer a comprehensive analysis of the current understanding of physical image quality metrics relevant to X-ray machines in pediatric interventional cardiology, taking into consideration the key factors reported in the literature that influence this outcome. The pertinent information gathered for this purpose is presented below, aligning with the research questions addressed in this study.

4.1. RQ 1: What are the primary physical image quality metrics commonly utilized for characterizing X-ray machines employed in fluoroscopy-guided pediatric interventional cardiac procedures, and what are the prevalent methods employed to measure these metrics?

Table 1 presents the most evaluated physical image quality metrics in the included studies, comprising N, SNR, SdNR, C, CNR, and HCSR. These metrics hold significant importance in characterizing the fluoroscopic systems used in pediatric interventional cardiology procedures and are detailed below:

4.1.1. Noise

In digital imaging techniques, brightness variations are attributed to statistical fluctuations in X-ray detection and the electronic chains of digital image receptors, rather than changes in radiation attenuation [18,19]. N in fluoroscopy-guided pediatric interventional procedures poses challenges in distinguishing structures and accurately determining their size [20]. Image degradation in fluoroscopic and cineangiography imaging is mainly caused by two factors: quantum noise, resulting from scattered photons interacting with objects in the X-ray beam, and electronic noise, which originates solely from the detector and remains constant regardless of radiation dose [21].

Among the evaluated articles, only one study reported this metric, conducted by Vañó *et al*. (2010) [6]. Their conceptual framework was adapted from the work published by Huda *et al*. (2003), focusing on digital mammography systems [22]. According to the Eq. 1. [6], lower standard deviation of pixel mean within the ROI corresponds to reduced image noise [20], leading to higher image quality.

4.1.2. SNR

Signal refers to the representation of the object of interest (e.g., an artery or stent) depicted in the image [23]. SNR serves as an integrative parameter directly related to image quality, encompassing essential aspects such as C, spatial resolution, and noise, all contributing to overall image quality [24].

 doi:10.20944/preprints202308.0657.v1

SNR plays a crucial role in evaluating images during pediatric interventional cardiology procedures, considering the influence of noise on image quality while quantifying the amount of signal relative to the surrounding tissue [11].

The signal is ideally directly related to the number of photons detected by the image receptor [25]. However, relying solely on the signal is insufficient for a comprehensive image quality assessment. Therefore, SNR is commonly employed to evaluate image quality in pediatric interventional cardiology procedures, as it considers the impact of noise on the image while accounting for statistical quantum fluctuations [11]. This parameter exhibits a direct correlation with the square root of the X-ray image receptor dose, allowing for the detection of changes in image quality. Notably, alterations in tube voltage or beam filtration influence the distribution of grey levels in an image [7,11].

Most articles that addressed SNR calculated it using Eq. 2. They conducted SNR measurements on the TOR 18FG test object [26], comparing the brightness levels of a ROI situated in the first low-contrast disk and another in its vicinity. Onnasch *et al*. proposed a variant of this measurement by utilizing two distinct measures of SNR, namely SNRd and SNRb, which involved calculations in regions with high and low attenuation, respectively. Both SNRd and SNRb remained unaffected by linear grey level windowing, thus demonstrating their robustness as descriptors for image generation and detection quality [7]. However, it is worth noting that the single measurement approach predominated within the analyzed articles.

4.1.3. C

This metric represents the difference in signal (brightness level) between a structure of interest and its surroundings. In radiology, it is a relevant parameter because it is directly affected by the selection of the tube voltage (kV) and added filtration used in irradiation [27].

As shown in Table 1, the three articles that evaluated this metric used different test objects. However, based on Eq. 4, it is evident that the logic employed to position the ROIs was consistent, reflecting through this metric the ability to distinguish two structures that generate a similar level of X-ray attenuation [10–12].

4.1.4. CNR

This physical parameter assesses an imaging mode's capability to differentiate between various contrasts present in an acquired image and the inherent noise within that image. A higher CNR value indicates a greater ability to distinguish objects such as guide wires or stents within blood vessels. Calculating the CNR enables an objective evaluation of the visibility of these vessels against the background's quantum noise [9,11].

The three articles addressing CNR utilized different test objects and formulas, as seen in Eqs.4 and 5. This lack of consensus regarding the metric is noteworthy, despite the recognized importance of CNR in providing valuable insights into image quality and the ability to detect crucial details in the context of medical imaging, which of outmost importance in the context of pediatric interventional cardiology [9,11].

4.1.5. HCSR

Spatial resolution is the ability of an imaging system to represent two adjacent structures as independent elements, involving the recognition of the edge of the structures depicted in the image [19]. In digital systems, this parameter is inversely proportional to the size of the pixels in the array [28]. In techniques such as interventional radiology, a special form of spatial resolution is employed, which refers to the ability to recognize adjacent structures when they exhibit a high difference in attenuating capacity (such as a catheter inside a blood vessel). This is known as HCSR [17]. Additionally, in the context of optimizing radiographic procedures, it has also been used to assess differentiation between bone tissue and soft tissue [23], and to the ability to visualize small blood vessels [4].

 doi:10.20944/preprints202308.0657.v1

According to Table 1, all the articles included in this review evaluated the HCSR using a test object consisting of a bar pattern composed of groups of radiolucent and radiopaque bars grouped according to their spatial frequency (0.5 – 5.0 LP/mm) [1,4,6,8,11–13,17]. In general, three frames were evaluated per run, which helps reduce bias associated with the automatic exposure control (AEC) adjustment period in the initial frames [1]. Regarding the formula used to calculate HCSR (Eq. 6), there is complete consensus among the published articles.

Finally, another crucial parameter in this context, not addressed by the studies included in the present systematic review, is the Modulation Transfer Function (MTF). MTF is an alternative method for evaluating resolution, closely linked to detector properties, and has been reported in similar contexts within medical imaging [29], thus warranting consideration in this domain.

4.2. RQ 2: What factors have been examined in the literature for their impact on physical image quality metrics in characterizing X-ray machines used in fluoroscopy-guided pediatric interventional cardiac procedures?

4.2.1. PMMA thickness

Within this systematic review, the focus lies on the examination of PMMA thickness as a factor influencing image quality, particularly in relation to SNR (Table 1 and Table 2). Several studies analyzed the correlation between SNR and the thickness of irradiated PMMA. Vañó *et al*. characterized a pediatric biplane angiographic system with image intensifier (II) technology and observed a trend of decreasing SNR with increasing PMMA thickness (4, 8, 12, 16, and 20 cm) [11]. Similarly, three studies by Ubeda *et al*. yielded analogous trends when evaluating different devices [8]. Corredoira *et al*. evaluated the impact of PMMA thickness in a biplane angiographic system with flat panel detector (FPD) technology for pediatric interventional cardiology and reported SNR behavior consistent with previous findings [13]. Lubis *et al*. reported similar trends [5].

Furthermore, the investigation by Gislason *et al*. explored C in the cardiac catheterization laboratory, utilizing tin as a substitute for iodine-based contrast in an FPD system. The study involved PMMA thicknesses of 8.5, 12, and 16 cm to approximate typical pediatric patient chest sizes [10]**.** Vañó *et al*. examined the impact of increasing PMMA thicknesses (ranging from 4 to 20 cm in 4 cm intervals) on contrast in a biplane system equipped with an II system. The contrast showed a direct relationship with dose increase between each operating mode, except for one of them, where a fitting error was detected through system characterization [11]**.**

All studies reporting the HCSR analyzed the influence of PMMA thickness on this metric [1,4,6,8,11–13,17]**.** The results consistently indicated that as the PMMA thickness increased, the HCSR tended to decrease, primarily due to the influence of scatter radiation [13]**.**

Additionally, de las Heras *et al*. aimed to objectively evaluate image quality in digital subtraction angiography (DSA) using the IEC type B phantom [30], measuring CNR. They introduced two scores for overall image quality. CNR_{dif} measured the difference between maximum and minimum CNR values, assessing the X-ray system's ability to distinguish tissues with similar absorption properties. CNR_{sum} combined four CNR values, reflecting vessel visibility. Key findings showed low uncertainties for both metrics, facilitating the relationship between examination of physical and clinical image quality [8].

4.2.2. Operation mode

Operational modes are programs provided by the interventional cardiology equipment, defining various aspects of irradiation, and are determined by each manufacturer. Typically, interventional cardiology systems offer three fluoroscopy operational modes: low (FL), medium (FM), and high (FH) dose, along with a cine mode (CI) [5]. Properly adjusting the system in terms of dose should result in an increase in image quality as one transitions from one operational mode to the next [1]. According to Table 2, this factor represents the second most frequently reported variable, and the studies consistently demonstrate similar results, indicating a reduction in image quality in

 doi:10.20944/preprints202308.0657.v1

terms of HCSR. This reduction has been attributed to the increase in dose per frame, leading to a consequent reduction in quantum noise [1,4,11].

While the configuration of each mode may vary among systems, evidence suggests that evaluating image quality along with measuring dose levels can alert to system misalignments or malfunctions. For instance, Vañó *et al*. reported an inconsistency in the dose and image quality changes for the FM mode compared to the other operational modes, highlighting the need for adjustment in this mode [11].

4.2.3. Anti-scatter grid

The study conducted by Ubeda *et al*. analyzed the impact of using an anti-scatter grid on image quality in a biplane system based on II technology, considering four PMMA thicknesses (4, 8, 12, and 16 cm). The use of the anti-scatter grid resulted in an average 14% increase in SNR it also revealed that changes in HCSR are more noticeable with the grid's utilization, particularly in CI mode [4]. Similarly, the article by Bor *et al*. evaluated grid performance parameters in C, SNR and HCSR for digital fluoroscopic examinations. The reports results indicated that C and HCSR resulted to be better metrics than SNR to evidence differences between each type of grid evaluated [12].

The 2004 study by Onnasch *et al*. recommended the use of grids for all patients, including infants [7]. However, subsequent research suggested the need to use grids selectively, based on patient thickness and acquisition protocols [4], Additionally, these studies emphasized the significance of adjusting image contrast to remove grids in cases of critical radiation dose [12].

4.2.4. Tube voltage

Technical parameters of the examination, such as tube voltage, influence the intensity and energy of photons reaching the image receptor and, consequently, impact the SNR values [8]. In that sense, SNRb and SNRd exhibit different dependencies on X-ray voltage. SNRb shows higher values at low voltages but decreases rapidly with rising voltages. On the other hand, SNRd reaches its maximum at approximately 79 kV. Based on these metrics, specific voltage ranges are recommended for use in pediatric interventional cardiology procedures [7].

An inverse relationship between CNR values and tube voltage was observed, with CNR decreasing as tube voltage increased [10]. A similar trend was noted for HCSR in PMMA blocks thicker than 5 cm, although the rate of decrease became less pronounced with increasing thickness. The utilization of a grid in conjunction with a 5 cm thickness resulted in an increase in HCSR with higher tube voltages for all grids, and the HCSR of images obtained without grids showed a slight improvement [12].

4.2.5. Field of view

Regarding the field of view (FOV) size, it had a significant impact on signal capture. The combination of 48 cm and 42 cm FOVs in fluoroscopy mode improved SNR but reduced spatial resolution. Conversely, utilizing 32 cm and 22 cm FOVs with unbinned pixels maintained spatial resolution at the cost of lower SNR. Notably, the most substantial SNR difference between fluoroscopy and CI modes was observed with the 32 cm FOV, resulting in lower fluoroscopy SNR overall [13].

In terms of HCSR, this article also indicated that HCSR increases as the FOV decreases due to magnification using unbinned pixels. In CI mode, there was no observed increase in resolution as magnification was electronically performed from 48 to 32 cm FOV. For a 22 cm FOV and pediatric protocols, fluoroscopy mode provided higher resolution than CI mode, attributed to the differences in focal spot size according to the mode utilized [13]. In a similar vein, electronic magnification by changing the FOV from 22 to 16 cm significantly improved HCSR but also increased the entrance dose by a factor of 1.9 for CI mode in the evaluated system [11].

4.2.6. Vessel diameter

 doi:10.20944/preprints202308.0657.v1

Iodine contrast was used to assess SNR in vessels of different diameters. Generally, high SNR was achieved in all vessel sizes when imaged in HD mode with any iodine concentration. HD mode was recommended for superior image quality, but LD mode provided adequate image quality and may be suitable for routine use. Measuring SNR in 1 mm vessels was particularly challenging, but an increasing trend in detectability was observed. Hence, further analysis in small arterial vessels is warranted due to the vessel size in young patients [5].

4.2.7. Frames per second

Despite the reported increase in dose when modifying the frames per second from 15 to 30, minimal differences in SNR were observed in the obtained images. It is possible that another metric could better reflect the change in incident photons on the detector; however, caution must be exercised when interpreting this result as the article does not provide a statistical comparison between both conditions [5].

4.2.8. Contrast mode

The evaluated system had a post-acquisition filtration algorithm (referred to as 'low contrast' and 'high contrast' modes) for CI mode, which did not affect the radiological parameters and, therefore, the radiation dose. The evaluation showed a trend towards increased SNR values in the 'high contrast' mode. Nevertheless, similar to the previous point, the information obtained should be approached with caution as no statistical comparison is provided for this variable [5].

4.2.9. Fluoroscopic system

The study conducted by Vañó *et al*. (2010) revealed that noise values were 40% lower in image II-based systems compared to those using FPD systems across all evaluated thicknesses (4, 8, 12, and 16 cm). In terms of efficiency, FPD systems require approximately twice the dose of II-based systems to achieve the same SNR value. The FPD-based system exhibited superior performance in HCSR compared to II systems, showing higher HCSR values ranging from 6.7% to 21.3% for PMMA thicknesses of 8, 12, and 16 cm. These results were attributed to the differences between the technologies employed, with II systems utilizing charge-coupled devices (CCD) and FPD systems employing large arrays of amorphous silicon photodiodes and thin film transistors with CsI(Tl) scintillators [6].

It is noteworthy that in the past decade, there has been a growing adoption of FPD-based systems, resulting in the continued presence of older II-based systems in certain facilities. Accordingly, it has been proposed to enhance dose optimization during the transition from II to FPD systems [31]. In general, both types of systems offer advantages for pediatric interventional cardiology, encompassing enhanced ergonomics, patient access, C, and spatial resolution, as well as reduced patient radiation dose [6,15].

4.2.10. Matrix size

HCSR showed a notable decrease in reduced matrices, which could have implications for the clinical interpretation of archived images. This metric demonstrated a robust correlation with visual inspection using magnification on a computer screen, effectively eliminating observer subjectivity. Given the relevance of matrix size to image quality, it is essential to consider this factor when comparing studies for other variables. In Table 2, there is a predominance of image quality evaluations conducted on matrices of 512×512. Which has been mainly related to the use of reduced matrix sizes and image compression as a cost-effective approach for managing large image datasets [17].

4.2.10. Filter thickness

The SNR can be influenced by the amount of added filtration during irradiation, leading to a slight decrease in SNR [24].

Both SNRd and SNRb measurements showed different voltage dependencies. SNRb performed best at low voltages but declined as the voltage increased. In contrast, SNRd decreased at low voltages, resulting in the disappearance of signal difference between Copper (Cu) steps of the test object due to quantum noise at higher amplitudes [7].

4.2.11. Automatic exposure control program

In fluoroscopic machines, the Automatic Exposure Control (AEC) system often automatically selects the filtration, tube voltage, and tube charge settings [32]. The proper adjustment of the AEC is crucial for maintaining high image quality, particularly by utilizing the advanced tubes' high output. Onnasch *et al*. suggest configuring AEC programs to keep X-ray voltage within an optimal range (above 55 kV but not exceedingly approximately 77 kV) to prevent a decrease in SNRb. Different AEC programs should be tailored for pediatric cardiac angiography to optimize image quality for children of different ages [7].

4.3. Final remarks

One commonly considered parameter in articles on optimization is the Figure of Merit (FOM), which complements objective image quality information with the value of an estimated magnitude in the procedure, such as the entrance surface air kerma (ESAK). Therefore, this parameter aids in assessing the system's efficiency in terms of the ESAK used to form a radiological image and should be reported together with the evaluated metrics [1,2,5,6,8,10,13,15].

This comprehensive review highlights the importance of optimizing X-ray system configurations and dynamic FPD settings in pediatric cardiac interventional procedures, considering radiation dose levels and specific clinical needs. The utilization of image quality metrics, such as SNR, HCSR, C and CNR, plays a pivotal role in refining imaging parameters and making informed clinical decisions, ultimately leading to improved diagnostic accuracy and enhanced patient care. These metrics not only aid in quality control and technique/system comparison but also effectively reduce radiation exposure in pediatric patients. Personalized protocols based on image quality metrics can minimize fluoroscopy time while maintaining high image quality. Nevertheless, it's crucial to consider the specific context, as the direct applicability of these metrics may be limited for certain interventional devices. Overall, integrating image quality metrics into medical practice shows significant promise in optimizing pediatric patient dose and image quality, benefiting cardiac X-ray imaging, and advancing medical procedures in this field.

The systematic review's findings have clinical and practical implications for pediatric healthcare and clinical practice. By understanding the most used physical image quality metrics and their impact on image characteristics, clinicians can optimize imaging protocols and balance image quality and dose for pediatric interventional procedures.

4.4. Study limitations

The most important limitations in this systematic review were as follows. Firstly, the analysis included articles published within a 23-year period, which might have excluded more recent studies with relevant findings. Additionally, preprint studies and unpublished data were not considered, potentially leading to the omission of valuable information. Moreover, the review was limited to studies published in English and Spanish, which could introduce language bias and overlook relevant studies in other languages. The low number of eligible references was another limitation, especially given the broad range of metrics considered, some of which were scarcely reported in the literature.

Regarding the articles retrieved, certain studies utilized in-house phantoms that were not validated, raising concerns about the accuracy and reliability of the results obtained from these studies. Furthermore, some articles omitted essential information, such as the program used for extracting data from ROIs, the number of analyzed images, image matrix size, and color depth, which could impact the comprehensiveness of the analysis. Lastly, for some metrics, there was no consensus

on the formula to calculate image quality, leading to variations in approaches among studies. Consequently, the results may offer trends but require careful interpretation.

4.5. Future research directions

The future trends in pediatric interventional cardiology imaging research hold significant potential for enhancing the understanding of the field. Addressing the limitations identified in the systematic review, future studies should consider expanding the inclusion criteria to include more studies, thus providing a more comprehensive dataset for analysis. Additionally, researchers are encouraged to validate in-house phantoms before utilization to ensure the accuracy and reliability of results. Furthermore, comprehensive reporting of study details should be considered to improve the transparency and comparability of future investigations. To foster consistency and comparability across studies, the establishment of consensus guidelines or recommendations for calculating and reporting physicals image quality metrics is essential. Exploring and developing novel image quality metrics that consider the unique characteristics and imaging needs of pediatric patients could advance the field further. Future researchers should consider examining the relationship between image quality metrics and long-term patient outcomes in pediatric interventional cardiology to shed light on the impact of image optimization on patient care and safety.

5. Conclusions

The systematic review provided insight into the use of physical image quality metrics to characterize X-ray equipment in fluoroscopy-guided pediatric interventional cardiac procedures. The evaluation of N, SNR, C, CNR, and HCSR has provided valuable information on the factors influencing image quality and dose in pediatric interventions. By optimizing imaging parameters based on these metrics, clinicians can improve diagnostic outcomes, improve patient safety, and minimize radiation exposure for vulnerable pediatric patients. However, it is important to recognize that these metrics may not fully capture the clinical processes, as they do not account for the image visualization process and observer perception of image quality. Nevertheless, they offer a valuable approach to assessing image quality and enrich the quality assessment process, complementing human observer evaluations.

Author Contributions: Conceptualization, D.N., K.V. and K.W.; methodology, D.N. and K.V.; validation, D.N. and K.V.; formal analysis, D.N., K.V. and K.W.; investigation, D.N., K.V. and K.W.; resources, D.N., K.V. and K.W.; data curation, D.N. and K.V.; writing—original draft preparation, D.N.; writing—review and editing, D.N., K.V. and K.W.; visualization, D.N., K.V. and K.W.; supervision, D.N.; project administration, D.N.; funding acquisition, D.N. All authors have read and agreed to the published version of the manuscript.

Funding: This research and APC was funded by Research Directorate at the Universidad de Tarapacá, grant number 7726-22.

Institutional Review Board Statement: Not applicable.

Informed Consent Statement: Not applicable.

References

1. Ubeda, C.; Salazar, L.; Retana, V.; Santos, F.; Salvador, L.; Sáenz, C.; Quesada, C.; Gavarrete, M.; Picado, M.; Arce, L. Characterization and Experimental Measurements of Scatter Dose at Cardiologist's Eyes during Paediatric Interventional Cardiology Procedures in Costa Rica. *Radiat Prot Dosimetry* **2017**, *176*, 450–455, doi:10.1093/rpd/ncx031.
2. Ubeda, C.; Miranda, P.; Dalmazzo, D. Evolution of Radiation Dose and Image Quality in a Pediatric Interventional Cardiology System [Dosis de Radiación y Calidad de Imagen En Un Equipo de Cardiología Intervencionista Pediátrico]. *Interciencia* **2014**, *39*, 518–523.
3. Azizmohammadi, F.; Navarro Castellanos, I.; Miró, J.; Segars, P.; Samei, E.; Duong, L. Generative Learning Approach for Radiation Dose Reduction in X-Ray Guided Cardiac Interventions. *Med Phys* **2022**, *49*, 4071–4081, doi:10.1002/mp.15654.

4. Ubeda, C.; Vano, E.; Gonzalez, L.; Miranda, P. Influence of the Antiscatter Grid on Dose and Image Quality in Pediatric Interventional Cardiology X-Ray Systems. *Catheterization and Cardiovascular Interventions* **2013**, *82*, 51–57, doi:10.1002/ccd.24602.
5. Lubis, L.E.; Bayuadi, I.; Pawiro, S.A.; Ng, K.-H.; Bosmans, H.; Soejoko, D.S. Optimization of Dose and Image Quality of Paediatric Cardiac Catheterization Procedure. *Physica Medica* **2015**, *31*, 659–668, doi:10.1016/j.ejmp.2015.05.011.
6. Vano, E.; Ubeda, C.; Martinez, L.C.; Leyton, F.; Miranda, P. Paediatric Interventional Cardiology: Flat Detector versus Image Intensifier Using a Test Object. *Phys Med Biol* **2010**, *55*, 7287–7297, doi:10.1088/0031-9155/55/23/007.
7. Onnasch, D.G.W.; Schemm, A.; Kramer, H.-H. Optimization of Radiographic Parameters for Paediatric Cardiac Angiography. *British Journal of Radiology* **2004**, *77*, 479–487, doi:10.1259/bjr/99356178.
8. Ubeda, C.; Vano, E.; Miranda, P.; Leyton, F.; Martinez, L.C.; Oyarzun, C. Radiation Dose and Image Quality for Paediatric Interventional Cardiology Systems. A National Survey in Chile. *Radiat Prot Dosimetry* **2011**, *147*, 429–438, doi:10.1093/RPD/NCQ463.
9. de las Heras, H.; Torres, R.; Fernández-Soto, J.M.; Vañó, E. Objective Criteria for Acceptability and Constancy Tests of Digital Subtraction Angiography. *Physica Medica* **2016**, *32*, 272–276, doi:10.1016/j.ejmp.2015.10.089.
10. Gislason, A.J.; Davies, A.G.; Cowen, A.R. Dose Optimization in Pediatric Cardiac X-Ray Imaging. *Med Phys* **2010**, *37*, 5258–5269, doi:10.1118/1.3488911.
11. Vano, E.; Ubeda, C.; Leyton, F.; Miranda, P. Radiation Dose and Image Quality for Paediatric Interventional Cardiology. *Phys Med Biol* **2008**, *53*, 4049, doi:10.1088/0031-9155/53/15/003.
12. Bor, D.; Birgul, O.; Onal, U.; Olgar, T. Investigation of Grid Performance Using Simple Image Quality Tests. *J Med Phys* **2016**, *41*, 21–28, doi:10.4103/0971-6203.177280.
13. Corredoira, E.; Vañó, E.; Alejo, L.; Ubeda, C.; Gutiérrez-Larraya, F.; Garayoa, J. Biplane Interventional Pediatric System with Cone-Beam CT: Dose and Image Quality Characterization for the Default Protocols. *J Appl Clin Med Phys* **2016**, *17*, 357–376, doi:10.1120/jacmp.v17i4.5828.
14. Vassileva, J.; Vano, E.; Ubeda, C.; Rehani, M.; Zotova, R. Impact of the X-Ray System Setting on Patient Dose and Image Quality; a Case Study with Two Interventional Cardiology Systems. *Radiat Prot Dosimetry* **2013**, *155*, 329–334, doi:10.1093/RPD/NCT011.
15. Page, M.J.; McKenzie, J.E.; Bossuyt, P.M.; Boutron, I.; Hoffmann, T.C.; Mulrow, C.D.; Shamseer, L.; Tetzlaff, J.M.; Akl, E.A.; Brennan, S.E.; et al. The PRISMA 2020 Statement: An Updated Guideline for Reporting Systematic Reviews. *BMJ* **2021**, *372*, doi:10.1136/BMJ.N71.
16. Kordolaimi, S.D.; Salvara, A.L.N.; Antonakos, I.; Tsalafoutas, I.A.; Broutzos, E.; Efstathopoulos, E.P. Comparative Performance Evaluation of a Flat Detector and an Image Intensifier Angiographic System Both Used for Interventional Cardiology Procedures in Adult and Pediatric Patients. *Physica Medica* **2013**, *29*, 178–187, doi:10.1016/j.ejmp.2012.02.001.
17. Vano, E.; Ubeda, C.; Geiger, B.; Martinez, L.C.; Balter, S. Influence of Image Metrics When Assessing Image Quality from a Test Object in Cardiac X-Ray Systems. *Journal of Digital Imaging 2010 24:2* **2010**, *24*, 331–338, doi:10.1007/S10278-009-9268-7.
18. Konstantinidis, A. Physical Parameters of Image Quality. *Comprehensive Biomedical Physics* **2014**, 49–63, doi:10.1016/B978-0-444-53632-7.00202-1.
19. Williams, M.B.; Krupinski, E.A.; Strauss, K.J.; Breeden, W.K.; Rzeszotarski, M.S.; Applegate, K.; Wyatt, M.; Bjork, S.; Seibert, J.A. Digital Radiography Image Quality: Image Acquisition. *Journal of the American College of Radiology* **2007**, *4*, 371–388, doi:10.1016/J.JACR.2007.02.002.
20. Morin, R.; Mahesh, M. Role of Noise in Medical Imaging. *Journal of the American College of Radiology* **2018**, *15*, 1309, doi:10.1016/J.JACR.2018.07.003.
21. Lamers, L.J.; Morray, B.H.; Nugent, A.; Speidel, M.; Suntharos, P.; Prieto, L. Multicenter Assessment of Radiation Exposure during Pediatric Cardiac Catheterizations Using a Novel Imaging System. *J Interv Cardiol* **2019**, *2019*, doi:10.1155/2019/7639754.
22. Huda, W.; Sajewicz, A.M.; Ogden, K.M.; Dance, D.R. Experimental Investigation of the Dose and Image Quality Characteristics of a Digital Mammography Imaging System. *Med Phys* **2003**, *30*, 442–448, doi:10.1118/1.1543572.
23. Nocetti, D.; Ubeda, C.; Calcagno, S.; Acevedo, J.; Pardo, D. Comparison of Image Quality among Three X-Ray Systems for Chest Radiography: First Step in Optimisation. *Radiat Prot Dosimetry* **2015**, *165*, 386–391, doi:10.1093/rpd/ncv081.
24. Ekpo, E.U.; Hoban, A.C.; McEntee, M.F. Optimisation of Direct Digital Chest Radiography Using Cu Filtration. *Radiography* **2014**, *20*, 346–350, doi:10.1016/J.RADI.2014.07.001.
25. Verdun, F.R.; Racine, D.; Ott, J.G.; Tapiovaara, M.J.; Toroi, P.; Bochud, F.O.; Veldkamp, W.J.H.; Schegerer, A.; Bouwman, R.W.; Hernandez-Giron, I.; et al. Image Quality in CT: From Physical Measurements to Model Observers. *Physica Medica* **2015**, *31*, 823–843, doi:10.1016/J.EJMP.2015.08.007.

26. TOR 18FG - Leeds Test Objects Available online: https://leedstestobjects.com/index.php/phantom/tor-18fg/ (accessed on 10 July 2023).
27. Doyle, P.; Martin, C.J.; Gentle, D. Application of Contrast-to-Noise Ratio in Optimizing Beam Quality for Digital Chest Radiography: Comparison of Experimental Measurements and Theoretical Simulations. *Phys Med Biol* **2006**, *51*, 2953, doi:10.1088/0031-9155/51/11/018.
28. Seeram, E. Dose Optimization in Digital Radiography. *Digital Radiography* **2019**, 213–227, doi:10.1007/978-981-13-3244-9_12.
29. Strauss, K.J. Pediatric Interventional Radiography Equipment: Safety Considerations. *Pediatr Radiol* **2006**, *36*, 126, doi:10.1007/S00247-006-0220-4.
30. IEC 61223-3-3:1996 | IEC Webstore Available online: https://webstore.iec.ch/publication/19374 (accessed on 20 July 2023).
31. Livingstone, R.S.; Chase, D.; Varghese, A.; George, P. V.; George, O.K. Transition from Image Intensifier to Flat Panel Detector in Interventional Cardiology: Impact of Radiation Dose. *J Med Phys* **2015**, *40*, 24–28, doi:10.4103/0971-6203.152241.
32. Konst, B.; Nøtthellen, J.; Bilet, E.; Båth, M. Radiographic and Fluoroscopic X-ray Systems: Quality Control of the X-ray Tube and Automatic Exposure Control Using Theoretical Spectra to Determine Air Kerma and Dose to a Homogenous Phantom. *J Appl Clin Med Phys* **2021**, *22*, 204, doi:10.1002/ACM2.13329.